Ab initio prediction of pressure-induced structural phase transitions of $CrVO_4$-type orthophosphates

S López-Moreno*
Facultad de Ciencias, Universidad Nacional Autónoma de México, Apdo. post. 70-646, México D. F. 04510, México

D. Errandonea
MALTA Consolider Team, Departamento de Física Aplicada-ICMUV, Universitad de Valencia, Edificio de Investigación, c/Dr. Moliner 50, Burjassot, 46100 Valencia, Spain

(Received 31 July 2012; published 25 September 2012)

In this work we present a theoretical study of structural stability of $CrVO_4$-type orthophosphates $InPO_4$ and $TiPO_4$ at ambient and high pressures. Total energy calculations and lattice dynamics were used to obtain structural and vibrational properties of these compounds. Also, we have studied at ambient pressure the orthophosphates $TlPO_4$ and VPO_4 in order to compare their structural and vibrational properties with $InPO_4$ and $TiPO_4$. Here we analyze the variation of the Raman and IR frequencies as functions of the reduced mass. Using the phonon dispersion relations we have calculated the Gibbs free energy and evaluated the phase transitions at 300 K, at which most experimental measurements are performed. By taking into consideration the Bastide's diagram and previous theoretical and experimental studies in APO_4 compounds, we have considered 12 candidate structures for the high-pressure regime. We found the following sequence for pressure-driven structural transition: $CrVO_4$ type $\rightarrow$ zircon $\rightarrow$ scheelite $\rightarrow$ wolframite, for $InPO_4$ and $TiPO_4$. The equations of state, phonon frequencies, and their behavior with pressure of the most stable polymorphs are also reported. We also included the phonon spectrum and the projected phonon density of states of each phase for both compounds. Finally, calculation of the evolution of magnetic moment is reported for $TiPO_4$.

DOI: 10.1103/PhysRevB.86.104112 PACS number(s): 61.50.Ks, 63.20.dk, 64.60.−i

I. INTRODUCTION

The crystal structure and physicochemical properties of $CrVO_4$-type oxides have been studied over the past five decades.[1] These compounds include orthophosphates $InPO_4$, $TiPO_4$, $TlPO_4$, and VPO_4 among others[2,3] as well as vanadates[4] and silicates, e.g., $TiSiO_4$.[5] They have an orthorhombic crystal structure [space group (SG) *Cmcm*, No. 63, $Z = 4$] which is comprised of nearly regular edge-sharing octahedra of AO_6 (A = In, Ti, Tl, or V). In addition, the P atoms occupy the tetrahedral interstitial sites constructed by cubic close-packed oxygen atom arrays. Figure 1(a) illustrates the crystalline structure. There, it can be seen that the TiO_6 (InO_6) octahedra form chains that propagate in the c axis, with these chains linked to one to another by PO_4 tetrahedra. These tetrahedra share corners with the octahedral units of the chains.

In addition to the magnetic properties,[6] phosphates crystallizing in the $CrVO_4$-type structure are interesting because this structure is intermediate between quartz-like structures with only fourfold-coordinated cations and structures with both cations in sixfold coordination. In particular, crystal chemistry arguments[7–9] predict that, under compression, these phosphates will undergo phase transitions to crystal structures where sixfold coordinated phosphors can be achieved.[10] Additional interest in these compounds comes in connection with Li ion batteries[11] since they are delithiated forms of cathode materials. Finally, some attention has been dedicated to $CrVO_4$-type phosphates because they can be formed by oxidation on the surface of phosphide semiconductors.[12]

Given the close connection of $CrVO_4$-type phosphates with quartz-like phosphates, a high-pressure study of the structural and vibrational properties of $InPO_4$ and $TiPO_4$ is quite attractive from the structural systematic point of view. Unfortunately, in contrast with other binary oxides such as zircons,[13,14] wolframites,[15] monazites,[16] scheelites,[17] barites,[18] and berlinites,[19] no high-pressure studies have been performed yet in $CrVO_4$-type oxides. The aim of our research is to investigate the physical properties of $InPO_4$ and $TiPO_4$ at high pressure. In order to do it, we performed density-functional theory (DFT) calculations of the crystal total energy as a function of the volume. Due to the fact that calculations are performed at 0 K, we used also the quasiharmonic approximation based on the calculated phonon frequencies[20] in the whole Brillouin zone (BZ) to search for the minimum Gibbs free energies at a temperature of 300 K.

Upon compression, phase transitions are predicted to take place to the zircon, scheelite, and wolframite structures. The low-pressure phases are more compressible than those of other phosphates, having a bulk-modulus (B_0) smaller than 80 GPa, but the high-pressure phases show considerably smaller compressibilities. For $InPO_4$ ($TiPO_4$), no evidence of sixfold coordinated phosphors is found up to 47.8 (49.3) GPa, when the high-pressure scheelite-type phase undergoes a structural transformation to the wolframite-type phase.

The paper is organized as follows: In the next section, we give a detailed description of the computational procedure. The crystal structures from the most representative phases of $InPO_4$ and $TiPO_4$ are briefly described in Sec. III. The results from $CrVO_4$-type structures and vibrational frequencies are presented in Secs. IV A and IV B, respectively. The high-pressure phases and their lattice dynamics are presented in Secs. IV C and IV D, respectively. The results from post-scheelite high-pressure phases are in Sec. IV E. In Sec. IV F we report the magnetic behavior of $TiPO_4$ under pressure. Finally, we discuss and summarize the main results of this work in Sec. V.

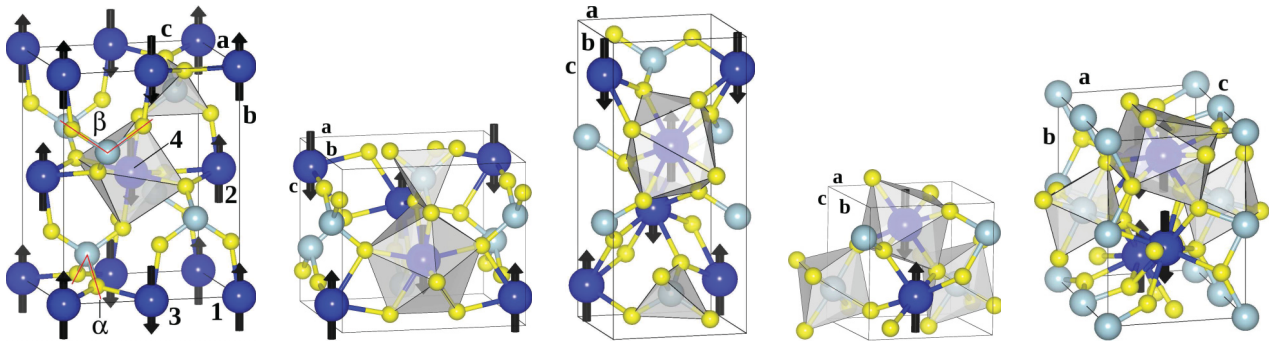

(a) $CrVO_4$-type (b) Zircon (c) Scheelite (d) Wolframite (e) $SrUO_4$-type

FIG. 1. (Color online) $CrVO_4$-type, zircon, scheelite, wolframite, and $SrUO_4$-type structures of APO_4 (A = V, Ti, In, Tl) compounds. Big blue circles: A atoms; medium cyan circles: P atoms; and small yellow circles: O atoms. The structures were drawn using the structural parameters of $TiPO_4$ at 0 GPa ($CrVO_4$ type), 15.5 GPa (Zircon), 23.5 GPa (Scheelite), 59.9 GPa (Wolframite), and 64 GPa ($SrUO_4$ type). The coordination numbers for the Ti or In (P) atom for $CrVO_4$-type structures, zircon, scheelite, wolframite, and $SrUO_4$-type structures are 6 (4), 8 (4), 8 (4), 6 (6), and 9 (6), respectively. Arrows indicate the direction of the magnetic moment of Ti atoms for the magnetic state of lowest energy. **a**, **b**, and **c** are the lattice parameters.

II. COMPUTATIONAL DETAILS

Calculations of the total energy are performed within the framework of the density functional theory (DFT) and the projector-augmented wave (PAW)[21,22] method as implemented in the Vienna *ab initio* simulation package (VASP).[23–26] We use a plane-wave energy cutoff of 520 eV to ensure a high precision in all our calculations. For the exchange correlation energy, we have used the generalized gradient approximation (GGA) in the Perdew-Burke-Ernzerhof (PBE)[27,28] prescription. However, while we found a good agreement with experimental results for the equilibrium volume, V_0, in $TiPO_4$ and VPO_4, the error in the values of V_0 for $InPO_4$ and $TlPO_4$ is $\approx$8%. Hence, we also made the calculations of V_0 for $InPO_4$ and $TlPO_4$ with AM05[29–31] and PBE for solids[32,33] (PBEsol) functionals. We found a better agreement with PBEsol functionals for these two compounds when comparing the results of V_0 obtained with PBE, PBEsol, and AM05 functionals. Thus, in what follows, the results reported here for the magnetic ($TiPO_4$ and VPO_4) and nonmagnetic ($InPO_4$ and $TlPO_4$) compounds were obtained with PBE and PBEsol exchange correlation functionals, respectively.

Due to Ti atoms presenting a magnetic moment, μ_{Ti}, one must consider the different magnetic configurations within the collinear magnetism for $CrVO_4$-type structures and high-pressure phases. As an example, consider the $CrVO_4$-type structure in Fig. 1(a). Here there are four Ti atoms in the unit cell with nonequivalent positions, so that there are one ferromagnetic (FM: $\uparrow\uparrow\uparrow\uparrow$) and three possible antiferromagnetic (AFM: $\uparrow\uparrow\downarrow\downarrow$, $\uparrow\downarrow\uparrow\downarrow$, $\uparrow\downarrow\downarrow\uparrow$) configurations. Similar calculations have be done in $TiPO_4$ to study the magnetic exchange couplings.[34]

A Monkhorst-Pack scheme is employed to discretize the Brillouin-zone (BZ) integrations[37] with meshes of $4\times3\times4$, $4\times4\times4$, $4\times4\times2$, $4\times4\times4$, $4\times3\times3$, $2\times3\times4$, and $4\times4\times1$, which correspond to sets of 8, 6, 4, 16, 8, 4, and 8 special k points in the irreducible BZ for *Cmcm*, zircon (SG: $I4_1/amd$, No. 141, $Z=4$), scheelite (SG: $I4_1/a$, No. 88, $Z=4$), wolframite (SG: $P/2c$, No. 13, $Z=2$), $SrUO_4$-type (SG: *Pbcn*, No. 60, $Z=4$), β-$InPO_4$ (SG: *Pnma*, No. 62, $Z=4$), and monoclinic distorted $CrVO_4$-type structures (SG: $P2_1/m$, No. 14, $Z=8$), respectively. For the additional structures considered in the high-pressure regime, we use the mesh most suitable for each case. In the relaxed equilibrium configuration, the forces are less than 3 meV/Å per atom in each of the Cartesian directions. The high degree of convergence for the calculated forces is required for the calculations of the dynamical matrix using the direct force constant approach (or supercell method).[38] The construction of the dynamical matrix at the Γ point is particularly simple and involves separate calculations of the forces in which a fixed displacement from the equilibrium configuration of the atoms within the unit cell is considered. The symmetry aids by reducing the number of such independent distortions to 24 independent displacements for the orthorhombic *Cmcm*, 14 for tetragonal zircon ($I4_1/amd$), 14 for the tetragonal scheelite ($I4_1/a$), 24 for the monoclinic wolframite, 30 for the orthorhombic $SrUO_4$ type, 30 for monoclinic β-$InPO_4$ phase, and 108 for monoclinic $P2_1/m$. Diagonalization of the dynamical matrix provides both the frequencies of the normal modes and their polarization vectors. It allows us to identify the irreducible representation and the character of the phonon modes at the zone center. The phonon dispersion curves are calculated along several high-symmetry directions in the BZ. The calculation of the phonon dispersion relation are done using the supercells $2\times3\times2$, $2\times2\times2$, and $2\times2\times1$ times the conventional unit cell for $TiPO_4$ *Cmcm*, $InPO_4$ *Cmcm* (zircon, scheelite, wolframite, $SrUO_4$ type, and β-$InPO_4$), and monoclinic $P2_1/m$, respectively. The dynamical matrices are obtained at the defined q points within the supercell and the other q points were fitted by using Fourier transform methods. The phonon dispersion curves are calculated along several high-symmetry directions in the BZ from the minimal set of dynamical matrices. The phonon density of states (PDOS) is obtained by integration of the phonon frequencies with a very high number of k points.

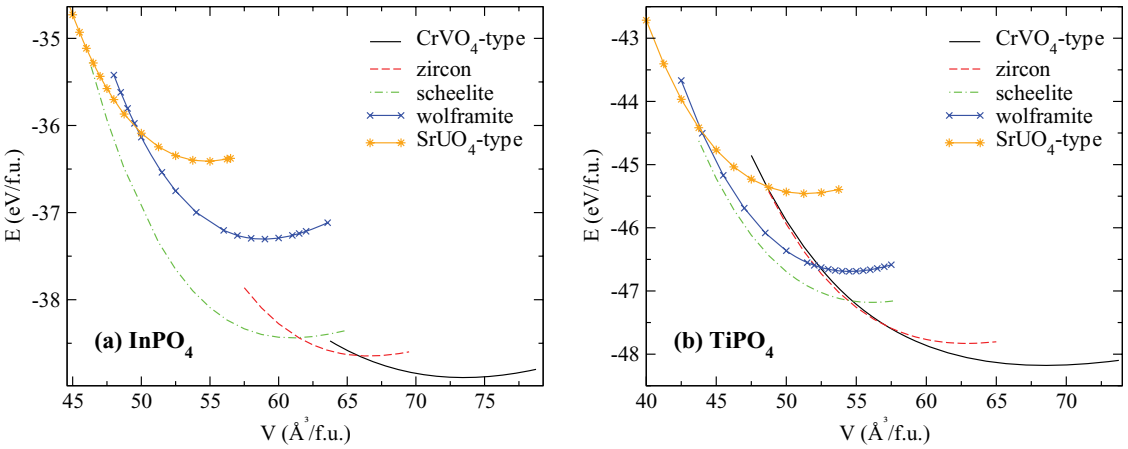

FIG. 2. (Color online) Calculated total energy-volume (per f.u.) curves for $CrVO_4$-type, scheelite, zircon, wolframite, and $SrUO_4$-type structures for (a) $InPO_4$ and (b) $TiPO_4$.

III. CRYSTAL STRUCTURES

For our theoretical study of the structural stability of $InPO_4$ and $TiPO_4$ at ambient and high pressures, we have taken into consideration previous results obtained in related compounds and the packing-efficiency criterion proposed by Bastide.[7] We have studied for each compound the relative stability of 12 candidate structures using the calculation method outlined in the previous section. In addition to the $CrVO_4$-type structure described in the introduction, we have considered the monoclinic $P2_1/m$ distorted $CrVO_4$-type structure reported for $TiPO_4$[39] and the orthorhombic β structure for $InPO_4$,[40] which is also a high-temperature phase of $MgSO_4$ and $CoSO_4$.[41] Other structures considered are zircon[13,14] and scheelite.[42] Both structures have been proposed as high-pressure phases of $TiSiO_4$.[5] They consist of AO_8 bisdisphenoids and PO_4 tetrahedra. Monazite (SG: $P2_1/n$, No. 14, $Z = 4$), a structure closely related to zircon and scheelite, has been also considered. These three structures imply an increase of the A cation coordination, but not change in P coordination. The wolframite[43,44] and high-pressure rutile-type (SG: $Cmmm$, No. 65, $Z = 2$) forms of $CrVO_4$ and $FeVO_4$[45] were also included in the calculations. In particular, these structures are interesting since imply a more efficient atomic packing and potential increase in the coordination of P. Another structure taken into account is the monoclinic $BaWO_4$-II-type structure (SG: $P2_1/n$, No. 14, $Z = 8$), which

TABLE I. Lattice parameters and Wyckoff positions (WPs) of $InPO_4$, $TiPO_4$, VPO_4, $TlPO_4$, and $TbPO_4$ at ambient pressure. The WPs of X, P, O(1), and O(2) atoms for $CrVO_4$-type compounds are 4a (0, 0, 0), 4c (0, y, 1/4), 8g (x, y, 1/4), and 8f (0, y, z), respectively. For $TbPO_4$ in the $I4_1/amd$ phase the WPs are 4a (0, 3/4, 1/8), 4b (0, 1/4, 3/8), and 16h (0, y, z), for Tb, P, and O, respectively.

	$InPO_4$		$TiPO_4$			VPO_4		$TlPO_4$		$TbPO_4$	
	NM	Expt.[a]	NM	AFM	Expt.[b]	AFM	Expt.[b]	NM	Expt.[a]	NM	Theor.[d]
a (Å)	5.3355	5.308	5.5004	5.4183	5.303	5.3090	5.232	5.4387	5.395	6.9949	6.9913
b (Å)	8.0454	7.851	8.1252	8.0851	7.902	7.9220	7.774	8.1312	8.010		
c (Å)	6.8255	6.767	5.9540	6.2317	6.349	6.2913	6.285	7.1455	7.071	6.0823	6.0823
V (Å^3)	293.0	282.0	266.1	273.0	266.05	264.60	255.63	316.0	305.56	297.60	297.29
$d_{A\text{-}O}$ (Å)	2.0818		1.9707	1.9646	1.950	1.9351	1.928	2.1457			
	2.2162		2.1170	2.1360	2.119	2.1059	2.080	2.3132			
$d_{P\text{-}O}$ (Å)	1.5216		1.5304	1.5318		1.5330		1.5309			
	1.5772		1.5772	1.5743		1.5755		1.5730			
μ_A (μ_B)				0.713	0.85[c]	1.801	1.81[c]				
B_0 (GPa)	78.65		100.65	72.93		79.16		53.57		128.87	128
B_0'	4.05		4.35	4.78		4.68		3.64		5.93	6.1
y(P)	0.3521	0.360	0.3478	0.3473	0.322	0.3484	0.3501	0.3535	0.358		
x(O1)	0.2603	0.240	0.2677	0.2630	0.235	0.2581	0.2408	0.2656	0.236		
y(O1)	0.4668	0.475	0.4616	0.4600	0.459	0.4636	0.4630	0.4668	0.470		
y(O2)	0.2538	0.246	0.2409	0.2402	0.260	0.2414	0.2430	0.2425	0.245	0.0762	0.0761
z(O2)	0.0596	0.062	0.0384	0.0472	0.046	0.0469	0.0509	0.0657	0.070	0.2156	0.2157

[a]Reference 2.
[b]Reference 35.
[c]Reference 3.
[d]The $TbPO_4$ is a zircon; Ref. 36.

has been considered as a post-scheelite phase of some AWO_4 compounds.[7] Furthermore, we considered the orthorhombic structures of $BaMnF_4$ type ($A2_1/am$, No. 36, $Z = 4$) and $SrUO_4$ type. These structures are located in the top of the northeast of Bastide's diagram, which makes them candidates for post-scheelite high-pressure phases. In particular, the $SrUO_4$ type was proposed as the high-pressure phase of $YAsO_4$[46] and $TbPO_4$.[36] Finally, the high-pressure (HP) monoclinic form of $AlPO_4$ has been also contemplated.[10] Structures such as berlinite,[19] barite,[18] anyhidrite,[47] and $AgClO_4$,[8] because they involve a decrease of cation coordination (an unusual occurrence upon compression) or dramatic change on the crystal structure, are not expected from the crystal chemistry point of view.[7]

IV. RESULTS AND DISCUSSION

A. Ambient pressure structures

In order to study the stability of $CrVO_4$-type orthophosphates at ambient pressure, we have considered the structures mentioned in previous section. Figure 2 shows the energy-volume curves for the most representative polymorphs of $InPO_4$ and $TiPO_4$. Our theoretical study indicates that the $CrVO_4$-type structure has the lowest free energy at ambient pressure for both compounds, which is in good agreement with experimental results.[2,35] According to the literature, $InPO_4$ is nonmagnetic (NM), whereas for $TiPO_4$ a magnetic order was observed by means of experiments[3] and *ab initio* calculations.[34] In order to describe the proper magnetic behavior of the $TiPO_4$ system, we performed collinear calculations with NM, FM, and AFM spin configurations. We found that the AFM ($\uparrow\uparrow\downarrow\downarrow$) configuration has the lowest energy; see Fig. 1(a). We will further discuss in Sec. IV B the thermodynamic stability of the NM phase compared to the AFM phase of $TiPO_4$ in the $CrVO_4$-type structure. The equilibrium lattice parameters were calculated by minimizing the crystal total energy obtained for different volumes. These lattice parameters were used to fit a third-order Birch-Murnaghan equation of state (EOS).[51] The results for the equilibrium volume V_0, bulk modulus B_0, bulk modulus pressure derivative B_0', magnetic moment of A cation per f.u., μ_A, lattice parameters a, b, and c, interatomic bond distances ($d_{A\text{-}O}$ and $d_{P\text{-}O}$), and WPs for $CrVO_4$-type orthophosphates are summarized in Table I.

To validate the accuracy of our theoretical parameters we have optimized the zircon phosphate $TbPO_4$, which has been previously studied by x-ray diffraction experiments and *ab initio* calculations.[36] We found that our results are in very good agreement with those from Ref. 36; see Table I.

As is reported in the literature, $InPO_4$ can also occur in the orthorhombic β phase,[40] which is also a high-temperature phase of $MgSO_4$ and $CoSO_4$,[41] whereas $TiPO_4$ can occur in a monoclinic $P2_1/m$ distorted $CrVO_4$-type structure.[39] We found that these phases are energetically nonstable compared to the $CrVO_4$-type structure of the respective compound. In the case of $TiPO_4$, we found that $P2_1/m$ has negative phonon modes at the Γ point.

Besides the experimental studies done in $InPO_4$[2] and $TiPO_4$[35] at ambient pressure, there is not much information in the literature about other orthophosphates with $CrVO_4$-type structure. In order to correlate our results with other compounds with this structure, we also study the orthophosphates $TlPO_4$[2] and VPO_4[35] at ambient pressure. For those we found that the $TlPO_4$ (VPO_4) is NM (AFM) like $InPO_4$ ($TiPO_4$). As shown in Table I, VPO_4 has the largest bulk modulus, B_0, followed by $InPO_4$, $TiPO_4$, and $TlPO_4$. These results are in good agreement with those for elastic properties.[52]

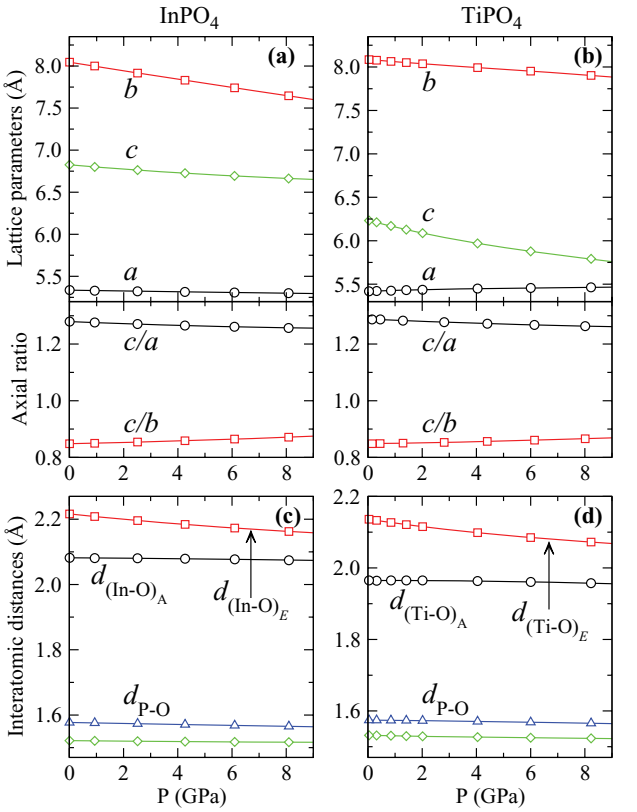

FIG. 3. (Color online) Pressure dependence of lattice parameters, axial ratio, and interatomic bond distances for $InPO_4$ and $TiPO_4$ in the $CrVO_4$-type structure.

According to Table I the equilibrium volume is overestimated by ≈2.6% for $TiPO_4$ (≈3.5% for VPO_4), as usual with the GGA approximation,[53] which implies that B_0 is underestimated by a similar proportion. For $InPO_4$ and $TlPO_4$, V_0 is overestimated by ≈3.8%. At the equilibrium volume, there are two interatomic bond distances, $d_{A\text{-}O}$, in the regular octahedra AO_6 [A = Ti, V, In, and Tl]. One distance is between A and the two axial O atoms, $d_{(A\text{-}O)_A}$, and the other is between A and the four equatorial O atoms, $d_{(A\text{-}O)_E}$. The larger interatomic bond distance belongs to the $d_{(A-O)_E}$; see Figs. 3(c) and 3(d). As seen in Table I, our results are in good agreement with the experimental data. Among the four phosphates, the NM $TlPO_4$ has the larger values of $d_{A\text{-}O}$ distances, and in general the NM phosphates have larger values than the AFM ones. In all the studied compounds, the octahedral distortion is reduced upon compression, as can be seen in Fig. 3. Regarding the tetrahedral PO_4, there also two $d_{P\text{-}O}$ bond distances. However, in this case these values are very similar for the four compounds. This means that lattice parameters and volumes of these orthophosphates are defined by the A cations and their $d_{A\text{-}O}$ distances with O atoms.

TABLE II. Calculated vibrational frequencies for $InPO_4$, $TiPO_4$, $TlPO_4$, and VPO_4 at zero pressure in the Γ point. The subindex AFM refers to the antiferromagnetic configuration. Frequencies ω are in cm^{-1} and pressure coefficients, $d\omega/dP$, are in cm^{-1}/GPa. The letters T, R, and ν_x refer to the translational, rotational, and internal (1: symmetric stretching; 2: symmetric bending; 3: asymmetric stretching; 4: asymmetric bending) phonon modes,[5] respectively.

	$InPO_4$				$TiPO_4$					$TlPO_4$	VPO_4
	ω	ω^a	$d\omega/dp$	γ	ω	ω_{AFM}	ω^b	$d\omega/dp$	γ	ω	ω_{AFM}
						Raman modes					
$T(B_{3g})$	159.12		1.83	1.05	185.00	170.96		1.80	0.90	142.61	190.11
$T(B_{1g})$	181.03	175	0.03	0.02	225.43	220.70		1.59	0.62	133.90	217.09
$R(B_{1g})$	238.41		1.00	0.39	279.67	262.49		2.64	0.23	203.62	261.89
$T(A_g)$	234.27	243	4.37	1.65	296.52	292.18		1.13	0.15	193.94	287.71
$R(B_{2g})$	288.08	303	4.85	1.52	307.73	311.70		4.41	1.19	239.81	275.94
$R(B_{3g})$	390.42		5.10	1.18	377.01	381.42		3.81	0.86	354.86	409.57
$\nu_2(A_g)$	407.40	416	0.45	0.10	434.05	430.99		0.85	0.17	375.04	448.03
$\nu_2(B_{2g})$	448.23	429	4.64	0.94	453.90	452.50		1.46	0.29	412.74	460.84
$\nu_4(B_{1g})$	510.24		1.69	0.30	527.56	527.72		0.23	0.05	479.69	525.76
$\nu_4(A_g)$	516.78	548	0.64	0.11	522.85	513.31		1.49	0.24	498.44	520.62
$\nu_4(B_{3g})$	638.97		3.47	0.50	630.10	626.26		1.39	0.20	612.85	648.38
$\nu_3(B_{1g})$	871.15	908	6.28	0.66	867.08	884.89		3.07	0.30	852.87	845.79
$\nu_3(A_g)$	912.91	950	5.44	0.55	884.49	891.73		3.23	0.02	887.29	899.47
$\nu_1(A_g)$	1007.71	1048	1.49	0.13	994.57	993.60		2.48	1.78	952.34	981.89
$\nu_3(B_{3g})$	1130.50	1164	4.02	0.33	1051.35	1061.25		3.96	2.35	1060.02	1065.36
						IR modes					
$T(B_{3u})$	106.21		−3.27	−3.07	228.27	207.85		2.94	1.80	27.35	211.19
$T(B_{1u})$	123.32		0.38	0.29	195.04	182.90		−7.46	−2.21	86.23	197.05
$T(B_{1u})$	171.36		3.28	1.72	231.14	225.23		2.60	1.06	134.83	265.70
$T(B_{2u})$	221.36		1.33	0.56	−202.95	303.46	285	0.65	0.47	154.35	317.80
$R(B_{3u})$	235.81		4.74	1.80	325.74	205.42		1.70	0.16	189.17	285.11
$T(B_{2u})$	289.55		0.53	0.16	356.23	362.54	350	−0.78	−0.19	236.68	383.92
$R(B_{1u})$	378.71		6.59	1.57	380.65	383.95	397	2.71	0.62	339.95	405.97
$\nu_2(B_{2u})$	447.20		2.69	0.55	461.54	457.01	467	2.44	0.46	413.41	486.79
$\nu_4(B_{3u})$	502.64		2.14	0.39	537.20	530.16	530	0.35	0.06	473.68	522.95
$\nu_4(B_{2u})$	514.61		0.55	0.10	529.99	525.46	559	1.60	0.27	496.97	520.65
$\nu_4(B_{1u})$	616.79		1.97	0.29	626.56	630.83	677	0.97	0.14	589.97	640.71
$\nu_3(B_{3u})$	888.29		6.18	0.64	853.40	868.78	948	3.24	0.32	878.18	866.04
$\nu_1(B_{2u})$	911.54		5.42	0.54	870.71	880.65	948	1.90	0.16	898.67	882.29
$\nu_3(B_{2u})$	1032.10		1.31	0.11	987.90	989.20	1015	2.64	2.48	984.30	968.68
$\nu_3(B_{1u})$	1093.11		3.45	0.29	999.71	994.87	1078	6.08	2.68	1045.11	982.73
						Silent modes					
A_u	86.86		−0.94	−1.03	229.27	207.72		1.52	0.16	39.13	201.32
A_u	207.99		2.74	1.20	237.61	234.07		4.46	2.03	175.23	247.65
A_u	464.28		6.75	1.32	435.79	423.31		1.88	0.08	432.39	430.75

[a]References 48 and 49.
[b]Reference 50.

Figures 3(a) and 3(b) show the evolution of the lattice parameters with pressure for $CrVO_4$-type structures of $InPO_4$ and $TiPO_4$, respectively. The pressure behaviors of interatomic bond distances in $InPO_4$ and $TiPO_4$ are shown in Figs. 3(c) and 3(d), respectively. According to Figs. 3(a) and 3(b), the c and b axes are more compressible than the a axis, for both compounds. However, $TiPO_4$ is more compressible in the c direction than $InPO_4$. The opposite occurs for the b axis. The axis a remains almost constant in the pressure range of Figs. 3(a) and 3(b). The behavior of lattice parameters with pressure can be explained in terms of the pressure dependence of interatomic bond distances of Figs. 3(c) and 3(d). First of all, it seems that only the $d_{(A\text{-}O)_E}$ bond distance has a significant change when pressure is applied, i.e., the main transitions in the $CrVO_4$-type structure are related to the AO_6 octahedra. When pressure is applied in the $CrVO_4$-type structure, the lattice parameter a remains almost constant due to absence of changes in the $d_{P\text{-}O}$ distances and in the angle α; see Fig. 1(a). However, the angle β becomes larger as pressure increases, which makes that AO_6 octahedra rotate in the (010) plane while the b and c lattice parameters becomes smaller due to the contraction in the $d_{(A\text{-}O)_E}$ bond distances. This behavior was observed for $InPO_4$ and $TiPO_4$ up to the pressure of their first phase transitions; see Sec. IV C.

B. Vibrational frequencies for ambient pressure structures

Regarding the vibrational properties, group theoretical considerations lead to the following vibrational representation at the Γ point for orthorhombic $CrVO_4$-type orthophosphates in standard notation:

$$\Gamma_O = 5A_g + 4B_{1g} + 6B_{1u} + 3A_u + 2B_{2g} + 7B_{2u} + 4B_{3g} + 5B_{3u},$$

where there are three acoustic modes ($B_{1u} + B_{2u} + B_{3u}$), the three silent modes A_u, 15 Raman active modes ($5A_g + 4B_{1g} + 2B_{2g} + 4B_{3g}$), and 15 IR active modes ($5B_{1u} + 6B_{2u} + 4B_{3u}$).

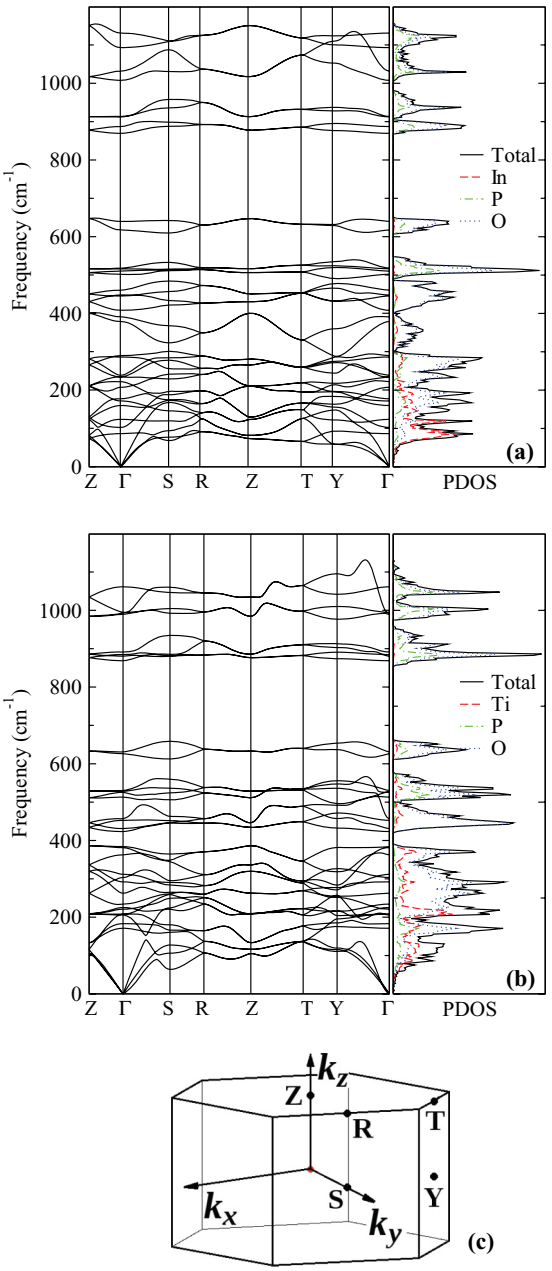

FIG. 4. (Color online) Phonon dispersion relation and phonon density of states (PDOS, in arbitrary units) of (a) $InPO_4$ and (b) $TiPO_4$ in the $CrVO_4$-type structure along the path of special k points Z-Γ-S-R-Z-T-Y-Γ at $P \approx 0$ GPa. (c) Brillouin zone for $CrVO_4$-type structure with the special k points used in (a) and (b).

The vibrational spectra can be interpreted in terms of modes of the PO_4 tetrahedra, which can be considered as independent units in the structures. Thus the modes can be classified either as internal (the PO_4 center of mass does not move) or as external (movements of PO_4 tetrahedra as rigid units). The translational modes (T) and the rotational modes (R) are considered to be external modes of the PO_4 tetrahedra and correspond to lowest frequencies. The internal modes of the PO_4 tetrahedra are ν_1 (symmetric stretching), ν_2 (symmetric bending), ν_3 (asymmetric stretching), and ν_4 (asymmetric bending).

Table II lists the calculated vibrational frequencies in therms of the previous assignment for the $CrVO_4$-type orthophosphates studied here. In the case of $InPO_4$ and $TiPO_4$ we also calculated the evolution of phonon modes with pressure to obtain the pressure coefficients ($d\omega/dp$) and Grüneisen parameters, $\gamma = \ln(\omega)/\ln(V)$.

To the best of our knowledge there is only one experimental report of infrared phonon frequencies for $TiPO_4$[50] and a few references of Raman phonon frequencies for $InPO_4$,[48,49,54] which are listed in Table II. However, the Raman frequencies of $InPO_4$ were obtained from porous InP (001) samples prepared by the application of high-voltage spark discharges.[49] In this case, the Raman frequencies corresponding to $InPO_4$ are from a superficial zone of InP. Also, it is important mention that the Raman spectrum of $InPO_4$ is sensitive to heat treatment due to the polymorphism in this material.[54]

In the previous section it was determined by total energy calculations that the AFM configuration is lower in energy than the NM one. In order to support this result, we also calculated the phonon frequencies for the NM phase of $TiPO_4$. According to Table II, in the NM phase of $TiPO_4$ there is a B_{2u} IR mode with a very negative frequency. We followed the behavior of phonon modes for this phase as a function of pressure and we found that this mode is negative up to 14 GPa. Thus, also it was demonstrated that the NM structure is nonstable compared

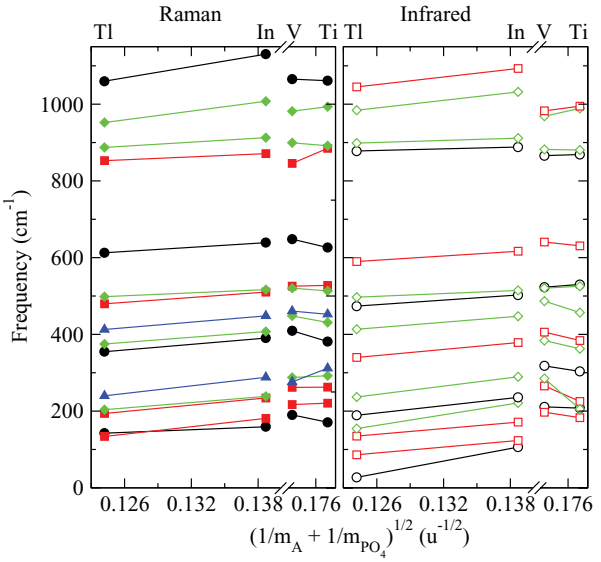

FIG. 5. (Color online) Trivalent-cation reduced-mass dependence of the Raman [A_g (♦), B_{1g} (■) B_{2g} (▲), and B_{3g} (●)] and infrared [B_{1u} (□), B_{2u} (◇), and B_{3u} (○)] frequencies at the Γ point for $InPO_4$, $TiPO_4$, $TlPO_4$, and VPO_4 $CrVO_4$-type structures at $P \approx 0$.

to the AFM structure from a thermodynamical point of view. According to Table II, the IR B_{3u} (106.21 cm^{-1}) and one A_u (6.86 cm^{-1}) from $InPO_4$ have negative pressure coefficients. For $TiPO_4$ the IR B_{1u} (182.90 cm^{-1}) and B_{2u} (362.54 $^{-1}$) also have negative pressure coefficients. As a general trend, the R and ν_3 phonon modes have the largest pressure coefficients among the the other T, ν_1, ν_2, and ν_4 modes.

The phonon dispersion relation and projected phonon density of states (PDOS) of $InPO_4$ and $TiPO_4$ in the $CrVO_4$-type structure along the path of special k points Z-Γ-S-R-Z-T-Y-Γ at $P \approx 0$ GPa are plotted in Figs. 4(a) and 4(b). As can be seen, the systems are dynamically stable with no imaginary phonon frequencies in the special k points from the Brillouin zone of Fig. 4(c). In the case of $TiPO_4$, we have to do the calculations with a $2 \times 3 \times 2$ supercell to get a good description of the phonon dispersion relation within the supercell approximation,[38] while for $InPO_4$ it was only necessary to use a $2 \times 2 \times 2$ supercell. This difference could be related to the long-range magnetic order of $TiPO_4$.[34] According to Figs. 4(a) and 4(b), $InPO_4$ and $TiPO_4$ present two phonon gaps around 600 and 650 cm^{-1}; also $TiPO_4$ has another one at 400 cm^{-1}. The PDOS of both compounds show that for frequencies bellow to 500 cm^{-1} the main vibrations belong to the AO_6 octahedra with a smaller contributions from PO_4 tetrahedra, whereas frequencies from 600 to 1150 cm^{-1} correspond to PO_4 tetrahedra.

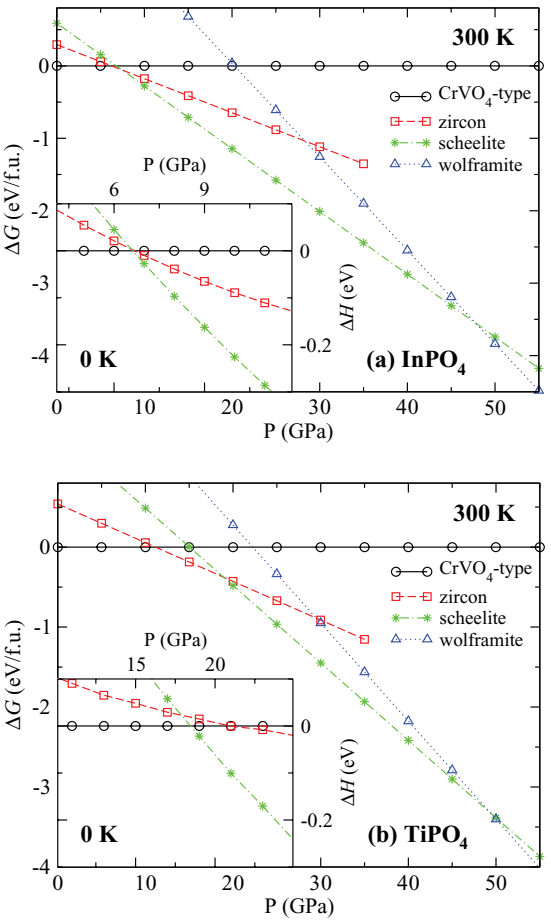

FIG. 6. (Color online) Gibbs free energy (at 300 K) as function of pressure curves for the most representative polymorphs of (a) $InPO_4$ and (b) $TiPO_4$. The Gibbs free energy is measured with respect to the Gibbs free energy of the $CrVO_4$-type structure. The inset shows the enthalpy (at 0 K) as a function of pressure. The enthalpy is also measured with respect to the enthalpy of the $CrVO_4$-type structure. According to the ΔG vs P plots of $InPO_4$ and $TiPO_4$, the phase transitions induced by pressure at 300 K occur as follows: $CrVO_4$ type → zircon → scheelite → wolframite, while at 0 K the ΔH vs P graphics indicates that transitions are from $CrVO_4$-type to scheelite phase.

According to Ref. 43, if we use the harmonic approximation, we can consider that the frequency of the oscillations is directly proportional to the inverse square root of the reduced mass of the cations. As in Ref. 43, we consider that our system consists of two separate blocks: the cation A and the polyanion PO_4. In order to identify some general trends of APO_4 $CrVO_4$-type phosphates, we plotted the Raman and IR frequencies of the different vibrational modes of the phosphates as a function of the inverse of the square root of the reduced mass μ of the A cation and the PO_4 polyanion ($1/\mu = 1/m_A + 1/m_{PO_4}$) in Fig. 5. In general, we found that magnetic phosphates ($TiPO_4$ and VPO_4) follow a different behavior than the nonmagnetic ones ($InPO_4$ and $TiPO_4$). While the nonmagnetic phosphates show an inverse proportional relationship between the frequencies of the phonon modes (Raman and IR) and the square root of the reduced mass μ, the AFM phosphates follows a behavior that depends on the frequency. With exception of B_{1g} and B_{2g} Raman modes, the slope of the reduced mass vs frequency changes from negative to positive at 650 cm^{-1}, which is the location of the phonon gap. It is worth mentioning that above 650 cm^{-1} all phonon modes are internal ν_x ($x = 1,2,3,4$), while below 400 cm^{-1}

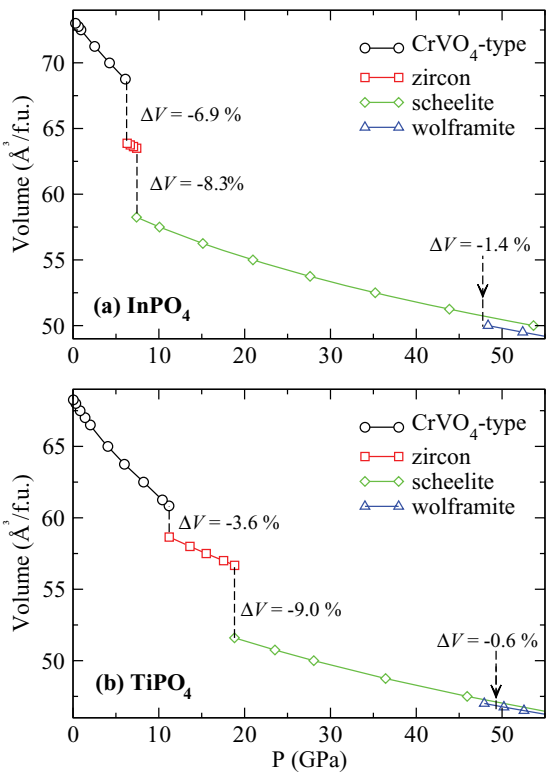

FIG. 7. (Color online) Pressure dependence of volume for the most representative phases of (a) $InPO_4$ and (b) $TiPO_4$. ΔV is the contraction volume at transition pressure.

TABLE III. Lattice parameters and Wyckoff positions (WPs) of $InPO_4$ and $TiPO_4$ in zircon, scheelite, and wolframite phases, at the pressure specified for each case.

	$InPO_4$			$TiPO_4$		
	Zircon	Scheelite	Wolframite	Zircon	Scheelite	Wolframite
P (GPa)	7.41	15.13	56.60	15.5	19.3	59.9
a (Å)	6.5711	4.5820	4.4269	6.3836	4.5394	4.1656
b (Å)	6.5711		4.9367			5.0348
c (Å)	5.8824	10.7167	4.5064	5.6441	9.9971	4.3627
β (deg)			95.68			89.88
V (Å^3)	254.0	225.0	98.0	230.0	206.0	91.5
$d_{A\text{-}O}$ (Å)	2.154 2.291	2.166 2.285	1.989 1.993 2.111	2.070 2.170	2.125 2.131	1.902 1.926 1.941
$d_{P\text{-}O}$ (Å)	1.541	1.544	1.559 1.689 1.742	1.530	1.548	1.583 1.664 1.711
B_0 (GPa)	147.82	164.3	212.24	143.0	190.16	234.74
B_0'	5.92	5.30	4.16	5.40	4.57	4.54
WPs						
A (x, y, z)	0 0.75 0.125	0 0.25 0.625	0.5 0.701 0.25	0 0.75 0.125	0 0.25 0.625	0.5 0.636 0.25
P (x, y, z)	0 0.25 0.375	0 0.25 0.125	0 0.159 0.25	0 0.25 0.375	0 0.25 0.125	0 0.140 0.25
O (x, y, z)	0 0.431 0.208	0.248 0.108 0.049	0.204 0.871 0.962	0 0.432 0.199	0.256 0.110 0.045	0.217 0.101 0.933
O (x, y, z)			0.232 0.377 0.379			0.230 0.357 0.392

almost all modes are external. So, between 400 and 650 cm^{-1} some phonon modes present important changes in the slope of the trend; see Fig. 5.

C. Pressure-driven transitions

In order to study the structural stability of orthophosphates $InPO_4$ and $TiPO_4$ at high pressures, we have considered the structures mentioned in Sec. III: $CrVO_4$ type, zircon, scheelite, wolframite, β-$InPO_4$, monoclinic distorted $CrVO_4$ type, monazite, rutile, $SrUO_4$ tpe, $BaMnF_4$ type, $BaWO_4$-II type, and the HP $AlPO_4$ ($P2_1/c$). Besides the importance of studying those phases based in their occurrence in other $CrVO_4$-type structures and orthophosphates at high pressures, it is a fact that are the best candidates which could be considered as high-pressure phases based on the packing-efficiency criterion proposed by Bastide.[7] In turn we propose that the phase transitions could be as follows: $CrVO_4$ type → zircon → scheelite → wolframite (or fergusonite) → orthorhombic (*Pnma*, *Pbcn*, *Pbca*) or monoclinic phase with space group number 14 → orthorhombic (*Cmca*, *Pbcm*, *Pnma*).

Figures 2(a) and 2(b) show the most representative energy-volume curves (per formula unit) for $InPO_4$ and $TiPO_4$, respectively, for which the relative stability and coexistence pressures of the phases can be extracted by the common-tangent construction.[53] It is clear that β-$InPO_4$, $P2_1/m$, monazite, rutile, $BaMnF_4$ type, $BaWO_4$-II type, and HP $AlPO_4$ ($P2_1/c$) are not competitive against the phases from Figs. 2(a) and 2(b). As shown in Figs. 2(a) and 2(b), the best candidates for high-pressure phases of $InPO_4$ and $TiPO_4$ are those in accordance with Bastide's diagram. Figures 6(a) and 6(b) show the evolution of Gibbs free energy with pressure for $CrVO_4$ type, zircon, scheelite, and wolframite for both compounds. The inset shows the enthalpy, ΔH, as function of pressure. In the case of $InPO_4$ it was observed in the pressure-enthalpy (ΔH vs P) diagram (at 0 K) that there is no phase transition from scheelite to wolframite (or $SrUO_4$) phase up to 80 GPa. In the ΔG vs P diagram (at 300 K) it was observed that the transition scheelite → wolframite must occur at a very high pressure. This implies that the transition wolframite → $SrUO_4$ could take place at further pressures. A similar behavior was observed for the $TiPO_4$ compound. The study of phase transitions at such very high pressures will be discussed in Sec. IV E. Thus, in what follows we only discuss the first two transitions.

At this point it is important to mention the general differences among the calculations done at 0 K by considering only the enthalpy, ΔH, and at 300 K with the Gibbs free energy, ΔG, obtained with the quasiharmonic approximation from the phonon dispersion relation in the whole Brillouin zone. At 0 K we found that the phase transition occurs from $CrVO_4$ type to scheelite phase for both compounds. At 300 K the transition is $CrVO_4$ type → zircon → scheelite, as it could be according to Bastide's diagram. This sequence in transition pressure was also observed in $TiSiO_4$.[5] However, for $TiSiO_4$ both transitions

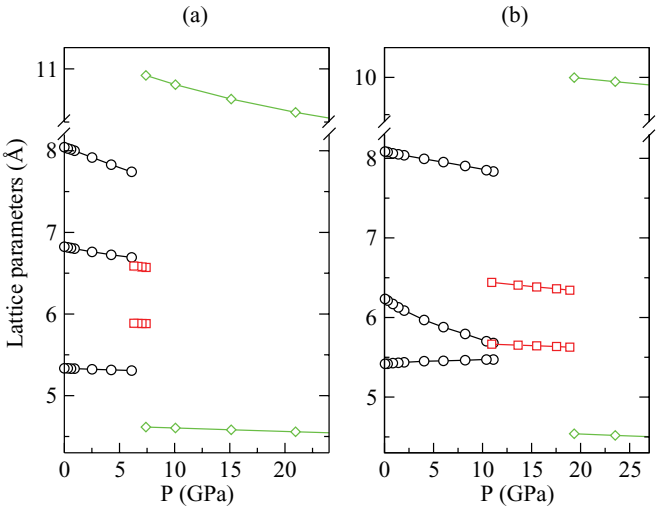

FIG. 8. (Color online) Lattice parameters as function of pressure of $CrVO_4$ type (○), zircon (□), and scheelite (◇), for (a) $InPO_4$ and (b) $TiPO_4$.

TABLE IV. Calculated vibrational frequencies for $InPO_4$ and $TiPO_4$ in the zircon (7.41 and 15.5 GPa, respectively) and scheelite (15.13 and 19.3 GPa, respectively) structures at the Γ point. Frequencies ω are in cm^{-1} and $d\omega/dP$ are in cm^{-1}/GPa. The letters T, R, and ν_x refer to the translational, rotational, and internal (1: symmetric stretching; 2: symmetric bending; 3: asymmetric stretching; 4: asymmetric bending) phonon modes,[42,55] respectively.

	Zircon							Scheelite					
	$InPO_4$			$TiPO_4$				$InPO_4$			$TiPO_4$		
	ω	$d\omega/dp$	γ	ω	$d\omega/dp$	γ		ω	$d\omega/dp$	γ	ω	$d\omega/dp$	γ
Raman modes													
$T(E_g)$	142.51	−1.16	−1.59	180.80	−0.81	−1.02	$T(E_g)$	143.81	0.89	1.38	255.59	0.78	0.89
$T(B_{1g})$	147.64	0.50	0.64	263.30	1.53	1.32	$T(B_g)$	163.62	1.52	2.03	261.09	0.85	0.94
$T(E_g)$	147.68	0.35	0.44	231.04	0.74	0.72	$T(E_g)$	283.54	1.78	1.38	321.40	2.24	1.99
$\nu_2(B_{2g})$	279.64	−0.48	−0.33	259.09	−1.06	−0.92	$T(B_g)$	296.59	3.46	2.53	402.23	2.83	2.02
$R(E_g)$	297.59	5.26	3.22	385.92	4.73	2.78	$R(A_g)$	300.19	1.25	0.92	352.33	1.34	1.10
$T(B_{1g})$	348.56	1.84	0.99	397.23	2.31	1.32	$R(E_g)$	408.47	2.41	1.30	436.22	2.21	1.46
$\nu_2(A_{1g})$	469.25	0.51	0.20	495.80	0.92	0.42	$\nu_2(A_g)$	444.83	1.29	0.65	432.45	1.66	1.12
$\nu_4(E_g)$	545.47	1.06	0.37	569.96	1.15	0.46	$\nu_2(B_g)$	474.18	1.25	0.59	504.01	1.84	1.06
$\nu_4(B_{1g})$	641.04	1.95	0.57	661.12	1.61	0.55	$\nu_4(E_g)$	578.43	2.14	0.82	621.13	1.87	0.88
$\nu_1(A_{1g})$	995.74	5.35	1.01	1051.78	4.39	0.94	$\nu_4(B_g)$	597.54	1.64	0.61	617.59	1.85	0.87
$\nu_3(E_g)$	1024.83	5.24	0.96	1061.02	4.19	0.89	$\nu_1(A_g)$	934.63	3.39	0.80	944.57	2.38	0.73
$\nu_3(B_{1g})$	1048.41	5.27	0.94	1145.75	4.65	0.92	$\nu_3(E_g)$	985.53	3.74	0.84	994.60	3.36	0.98
							$\nu_3(B_g)$	1001.04	3.87	0.86	984.70	2.84	0.84
IR modes													
$T(E_u)$	207.59	2.11	1.90	323.04	1.35	0.95	$T(A_u)$	177.77	4.20	4.92	325.97	3.17	2.75
$T(A_{2u})$	266.40	0.97	0.69	352.96	1.68	1.07	$T(E_u)$	179.47	0.55	0.69	271.70	0.22	0.24
$R(E_u)$	334.21	3.10	1.73	386.89	3.78	2.21	$R(E_u)$	337.42	2.14	1.40	395.96	3.29	2.36
$\nu_4(E_u)$	469.15	0.64	0.26	465.28	0.31	0.15	$\nu_4(A_u)$	424.95	−0.02	−0.01	405.07	−0.41	−0.30
$\nu_4(A_{2u})$	616.19	1.64	0.50	642.41	1.70	0.60	$\nu_4(E_u)$	536.60	1.03	0.43	543.04	1.09	0.59
$\nu_3(E_u)$	963.51	5.68	1.10	1019.66	4.25	0.94	$\nu_2(A_u)$	610.02	2.53	0.92	654.42	2.34	1.04
$\nu_3(A_{2u})$	1053.71	5.21	0.93	1129.44	4.43	0.89	$\nu_3(A_u)$	909.57	3.85	0.94	928.82	3.11	0.97
							$\nu_3(E_u)$	975.16	3.53	0.80	971.35	3.03	0.91
Silent modes													
$R(B_{1u})$	76.72	−8.64	−35.87	51.10	−7.00	−28.94	$R(B_u)$	348.19	1.84	1.17	428.95	1.12	0.76
$R(A_{2g})$	218.36	−0.33	−0.29	235.97	−0.23	−0.22	$\nu_2(B_u)$	557.88	3.69	1.45	625.26	2.97	1.37
$\nu_2(A_{1u})$	384.38	1.05	0.51	403.83	0.78	0.44	$\nu_1(B_u)$	922.75	3.17	0.76	939.03	2.70	0.84
$\nu_2(B_{2u})$	528.06	1.84	0.66	581.06	1.77	0.69							
$\nu_1(B_{2u})$	970.59	5.42	1.05	1022.09	4.26	0.94							

were observed bellow 4 GPa at 0 K by using only the enthalpy, ΔH. From this picture it is clear that it is necessary to use some approximation to obtain the Gibbs free energy to get a better description of a phase transition at temperatures $\neq$0 K; for example, the first-principles study done in $CeVO_4$, where the phase transitions described by experiments were only observed by considering the effect of temperature with the quasiharmonic approximation in the calculations.[56]

According to Fig. 6(a), as pressure increases up to 6.2 GPa there is a first-order phase transition in $InPO_4$ at 300 K from $CrVO_4$ type to the zircon phase. This transition involves a volume reduction, ΔV, of −6.9%; see Fig. 7(a). Upon further compression, the second phase transition zircon → scheelite take place at 7.5 GPa with a $\Delta V = -8.3\%$. We found that the scheelite phase is stable up to 47.8 GPa. The pressure dependence of volume for $InPO_4$ and $TiPO_4$ is shown in Figs. 7(a) and 7(b). For $TiPO_4$ the first and second transitions are at 11.1 and 18.9 GPa, with a ΔV of −3.6% and −9.0%, respectively. It is noteworthy that ΔV for the first transition in $InPO_4$ and $TiPO_4$ is smaller than the value of 11.8% observed in $TiSiO_4$ for the same transition.[5] The ΔV for the second transition is similar to that of $TiSiO_4$ (8.5%). As can be noted from Figs. 6(a) and 7(a), in $InPO_4$ the zircon phase is stable in a very short range of pressure at 300 K. The results from equations of state (EOS) of zircon and scheelite high-pressure phases of $InPO_4$ and $TiPO_4$ are listed in Table III. As seen, zircon and scheelite phases of $InPO_4$ and $TiPO_4$ have B_0 values which are smaller than in other ABO_4 phosphates.[57] In zircon and scheelite phases, the A (P) atoms have a coordination of 8 (4). The interatomic bond distances $d_{A\text{-}O}$ have larger values than in $CrVO_4$-type structures. Whereas the P atoms have only one d_{P-O} distance, which has an intermediate value to that observed in the $CrVO_4$-type structure of the respective compound; see Tables II and III.

Figure 8 shows the pressure dependence of the lattice parameters of $CrVO_4$-type and the high-pressure phases zircon and scheelite of $InPO_4$ and $TiPO_4$ compounds. As seen, lattice parameters c (from zircon) and a (from scheelite) are less compressible than the other a and c lattice parameters, respectively. A similar trend was observed for $TiSiO_4$.[5]

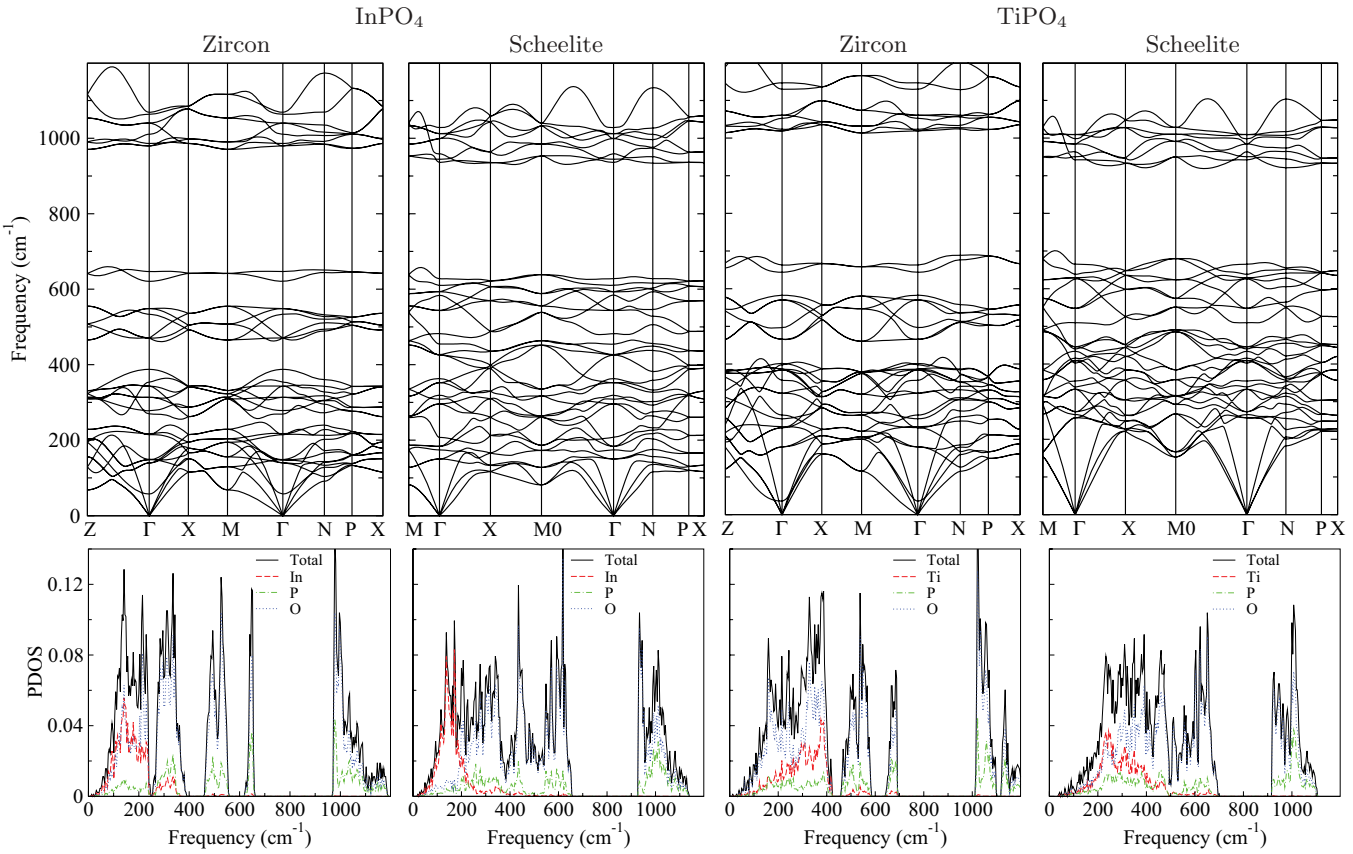

FIG. 9. (Color online) Phonon dispersion relation and PDOS (in arbitrary units) of $InPO_4$ and $TiPO_4$ in the zircon (7.41 and 15.5 GPa for $InPO_4$ and $TiPO_4$, respectively) and scheelite (15.13 and 19.3 GPa for $InPO_4$ and $TiPO_4$, respectively) structures along the path of special k points Z-Γ-X-M-Γ-N-P-X and M-Γ-X-M0-Γ-N-P-X, respectively. The special k points are illustrated in the Brillouin zones of Figs. 10(a) and 10(b).

Regarding the bulk modulus, $InPO_4$ and $TiPO_4$ have a similar value for zircon, while the scheelite phase of $TiPO_4$ is much less compressible than that of $InPO_4$. The values obtained for scheelite and zircon phases of $InPO_4$ and $TiPO_4$ are smaller than the values for rare-earth orthophosphates APO_4 (La, Nd, Eu, Gd, Er, Y, Tm)[57,58] and $TiSiO_4$.[5] However, these values are similar to those of $TbPO_4$.[36]

D. Lattice dynamics of the high-pressure phases: Zircon and scheelite

According to group theory, the tetragonal zircon phase has the following Γ phonon modes:

$$\Gamma_Z = 2A_{1g} + A_{1u} + A_{2g} + 4A_{2u} + 4B_{1g} + B_{1u} + B_{2g} + 2B_{2u} + 5E_u + 5E_g.$$

A and B modes are nondegenerate, whereas the E modes are doubly degenerate. Among these modes, there are 2 acoustic modes ($A_u + E_u$), 13 Raman active modes ($3A_g + 5B_g + 5\ E_g$), 7 infrared modes ($4E_u + 3A_{2u}$), and 5 silent modes ($B_{1u} + A_{2g} + A_{1u} + 2B_{2u}$).

Group theory predicts the following vibrational representation for the scheelite phase at the Γ point:

$$\Gamma_S = 3A_g + 5A_u + 5B_g + 3B_u + 5E_g + 5E_u,$$

where there are 2 silent modes ($A_u + E_u$), 13 Raman active modes ($5E_g + 5B_g + 3A_g$), 8 infrared modes ($4A_u + 4E_u$), and 3 silent modes ($3B_u$). Table IV lists the calculated vibrational frequencies, pressure coefficients, and Grüneisen parameters of zircon and scheelite phases from $InPO_4$ and $TiPO_4$. The phonon modes are described by using the same convention as for the $CrVO_4$-type structure of Table II. Unfortunately there is no information in the literature about Raman or IR phonon modes for high-pressure phases of the orthophosphates studied here. In the tetragonal zircon phase of both compounds there are several phonon modes [the Raman $T(E_g)$ and $\nu_2(B_{2g})$, and the silent $R(B_{1u})$ and $R(A_{2g})$] with negative pressure coefficients and Grüneisen parameters. The softening of $T(E_g)$ and $R(B_{2g})$ phonon modes was also observed in $TiSiO_4$[5] and $TbPO_4$,[36] while the softening of $R(B_{2g})$ was observed in $TmPO_4$[58] and $ScVO_4$,[60] to name a few.

As is well known, many compounds with scheelite-type structure present the usual softening of the $T(B_g)$ Raman active mode, which is related to the soft-mode theory of second-order phase transitions.[61] It is worth mentioning that this behavior was also reported for $TiSiO_4$,[5] $TbPO_4$,[36] and $ScVO_4$.[60] In our results, we did not find any phonon mode with negative pressure coefficient in $InPO_4$ and $TiPO_4$ for the scheelite phase; see Table IV. As a general trend, it is observed that in the zircon structure of both compounds the pressure coefficients are larger

than in scheelite, mainly in the ν_1 and ν_3 internal modes. In the zircon phase the $R(B_{1u})$ silent mode has the larger negative pressure coefficients: -8.64 for $InPO_4$ and -7.0 for $TiPO_4$. This is reflected in the large negative value of the Grüneisen parameter; see Table IV.

The phonon dispersion relations and PDOS of $InPO_4$ and $TiPO_4$ in the zircon (7.41 and 15.5 GPa for $InPO_4$ and $TiPO_4$, respectively) and scheelite (15.13 and 19.3 GPa for $InPO_4$ and $TiPO_4$, respectively) phases along the path of special k points Z-Γ-X-M-Γ-N-P-X and M-Γ-X-M0-Γ-N-P-X are plotted in Fig. 9. The Brillouin zones for zircon and scheelite are in Figs. 10(a) and 10(b). As is expected from the mass relation of In and Ti atoms, the branches of acoustic phonon modes are more dispersive in $TiPO_4$ than in $InPO_4$; see Fig. 9. This behavior could be understood by looking at the PDOS of both compounds, where the main states from In (Ti) are below 250 (400) cm^{-1}.

E. Post-scheelite high-pressure phases

According to the Bastide's diagram and previous high-pressure studies on ABO_4 compounds,[7] the wolframite, $BaWO_4$-II-, $BaMnF_4$-, $NaAlF_4$-, $KAlF_4$-, and $SrUO_4$-type structures, among others, could be considered as candidates for post-scheelite highpressure phases. One feature that these structures have in common is that the B cation has a coordination of 6; see the wolframite and $SrUO_4$-type structures in Figs. 1(d) and 1(e), respectively. In our study we have considered these structures as post-scheelite phases. According to Fig. 2 the most competitive phases are wolframite and $SrUO_4$-type phases. In the enthalpy vs pressure, ΔH vs P, graphic of $TiPO_4$ the transition scheelite → $SrUO_4$ type occurs at 79.1 GPa. However, we calculated the phonon structure of the $SrUO_4$-type phase at several pressures (from 45 to 82 GPa) and we found that there are several negative phonon modes at the Γ point, a clear indication of instability. On the other hand, there is no transition scheelite → wolframite in the ΔH vs P diagram, but in the ΔG vs P diagram at 300 K the transition occurs at 49.3 GPa; see Fig. 6(b). At this pressure we observed a volume reduction of $\Delta V = -0.6\%$, as shown in Fig. 7(b). A similar behavior in the ΔH vs P diagram is observed for $InPO_4$. However, the transition scheelite → $SrUO_4$ type occurs at 86.7 GPa. In the ΔG vs P diagram, at 300 K, the transition scheelite → wolframite happens at 47.8 GPa with $\Delta V = -1.4\%$; see Figs. 6(a) and 7(a). Note that a transition to a wolframite-type phase has been recently reported[62] to occur according to preliminary results presented by Stavrou *et al*. This result is apparently in agreement with our calculations, suggesting that sixfold-coordinated phosphor appears in $TiPO_4$ under extreme compression.

As can be seen in the structure of wolframite from Fig. 1(d), Ti (In) and P atoms have a coordination of 6. At 56.6 (59.9) GPa the interatomic bond distance $d_{P\text{-}O}$ in $InPO_4$ ($TiPO_4$) ranges from 1.559 (1.583) to 1.742 (1.711) Å, whereas $d_{In\text{-}O}$ ($d_{Ti\text{-}O}$) range from 1.989 (1.902) to 2.1111 (1.941) Å; see Table III. As can be deduced from the interatomic bond distances, the polyhedral TiO_6 and PO_6 are more irregular than in $CrVO_4$-type, zircon, and scheelite structures. From Tables I and III, it seems that this phase has larger values of bulk modulus than $CrVO_4$-type, zircon, and scheelite phases, due to the more efficient packing of atoms. Wolframite from $TiPO_4$ is the less compressible phase with a value of $B_0 = 234.74$ GPa, while in wolframite of $InPO_4$ $B_0 = 212.24$ GPa. Also, these values are larger than those observed for other

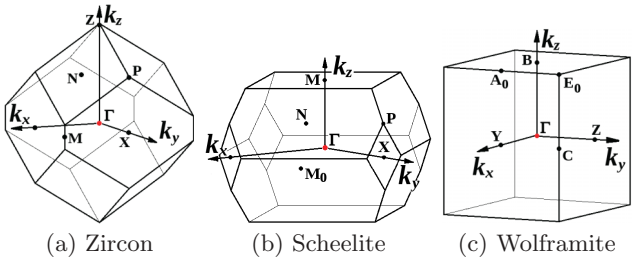

(a) Zircon (b) Scheelite (c) Wolframite

FIG. 10. (Color online) Brillouin zone from (a) zircon, (b) scheelite, and (c) wolframite structures.

TABLE V. Calculated vibrational frequencies for $InPO_4$ and $TiPO_4$ in wolframite at 56.6 and 59.9 GPa, respectively, at the Γ point. Frequencies ω are in cm^{-1} and $d\omega/dP$ are in cm^{-1}/GPa.

	$InPO_4$			$TiPO_4$		
	ω	$d\omega/dp$	γ	ω	$d\omega/dp$	γ
			Raman modes			
B_g	104.48	−0.33	−1.34	216.39	1.14	2.49
B_g	181.60	0.62	1.43	303.16	0.43	0.68
A_g	189.54	0.37	0.81	298.89	3.82	5.82
B_g	286.65	0.83	1.21	321.91	0.75	1.11
A_g	316.17	−0.24	−0.32	397.26	11.57	14.07
B_g	404.67	1.17	1.21	480.66	0.68	0.68
B_g	458.44	1.24	1.13	497.84	1.14	1.09
A_g	468.75	0.32	0.28	562.12	−1.04	−0.88
A_g	529.09	1.04	0.82	600.24	1.81	1.43
A_g*	581.50	1.72	1.23	654.52	1.64	1.23
B_g	638.31	1.47	0.96	612.32	1.81	1.41
B_g	681.24	1.96	1.20	705.16	2.01	1.35
B_g	744.18	1.87	1.05	788.62	1.75	1.06
A_g*	771.61	1.70	0.92	715.53	4.18	2.74
B_g*	994.47	3.09	1.30	913.84	2.59	1.34
A_g*	1018.09	2.21	0.90	947.17	4.53	2.25
B_g*	1071.16	2.50	0.98	1003.01	2.66	1.26
A_g*[a]	1101.92	2.91	1.10	1143.35	6.29	2.78
			IR modes			
B_u	123.62	−1.05	−3.56	252.19	−0.25	−0.47
A_u	228.84	0.29	0.54	392.89	0.57	0.69
B_u	242.51	0.79	1.35	386.55	0.47	0.59
A_u	391.62	0.53	0.57	473.72	0.38	0.38
B_u	417.14	0.71	0.72	450.30	0.66	0.70
B_u	523.85	1.50	1.20	549.97	1.75	1.51
A_u	530.06	0.41	0.32	608.72	1.03	0.81
B_u	614.26	1.55	1.06	655.99	1.84	1.33
A_u	730.27	1.95	1.11	681.84	1.45	1.01
B_u	741.15	1.81	1.02	728.04	1.97	1.28
A_u	788.05	1.72	0.91	779.24	2.11	1.29
B_u	798.16	1.80	0.94	821.68	1.98	1.14
A_u	830.25	2.57	1.29	818.64	2.53	1.46
B_u	997.11	3.19	1.33	931.69	3.04	1.55
A_u	1022.19	2.90	1.18	1033.77	2.85	1.31

[a]Stretching modes (Ref. 59).

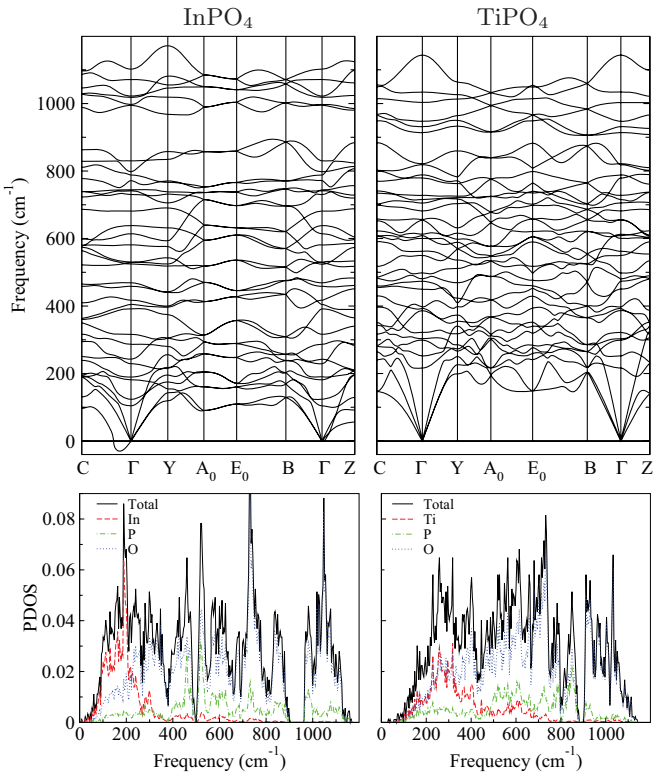

FIG. 11. (Color online) Phonon dispersion relations and PDOS (in arbitrary units) of $InPO_4$ and $TiPO_4$ in the wolframite structures along the path of special k points S-Γ-X-U-R-Z-Γ-Y.

AWO_4 wolframites (A = Mg, Zn, Mn, Cd),[15,63] which have values of B_0 between 130 and 160 GPa.

According to group theory, the monoclinic wolframite phase has the following Γ phonon modes:

$$\Gamma_V = 8A_g + 10B_g + 8A_u + 10B_u.$$

Here $2B_u$ and one A_u infrared modes are acoustic, 18 are Raman ($8A_g + 10B_g$) and 15 are infrared ($7A_u + 9B_u$). The frequencies, pressure coefficients, and Grüneisen parameters for both compounds are listed in Table V. In this phase of $InPO_4$, the modes B_g, A_g, and B_u soften with pressure. This B_u IR mode also softens in other compounds with wolframite structure.[43,59,64] Figure 11 shows the phonon spectrum along the path of special k points S-Γ-X-U-R-Z-Γ-Y, and the PDOS (in arbitrary units) of $InPO_4$ and $TiPO_4$. In Fig. 10(c) we show the Brillouin zone for the wolframite structure. We have calculated the phonon spectrum of $InPO_4$ in the wolframite structure from 37 to 66 GPa in intervals of ≈3.5 GPa, and we found that for all this range of pressure the acoustic B_{1u} IR mode softens between the C and Γ points. Below 52 GPa this mode softens in a site between the Γ and Z points. In wolframite $TiPO_4$, the acoustic A_u IR mode softens in the same points as the acoustic B_{1u} IR mode from $InPO_4$. Bellow 48 GPa, the acoustic B_{1u} IR mode from $TiPO_4$ also softens in a point between C and Γ. Contrary to the observation in $InPO_4$, in $TiPO_4$ the phonon spectrum of wolframite has no negative branches from 59 to 68 GPa, which is the higher pressure studied for the phonon spectrum. Regarding the PDOS, there is a small gap in comparison with the other phases around 900 cm^{-1}. There are many more branches due to the low

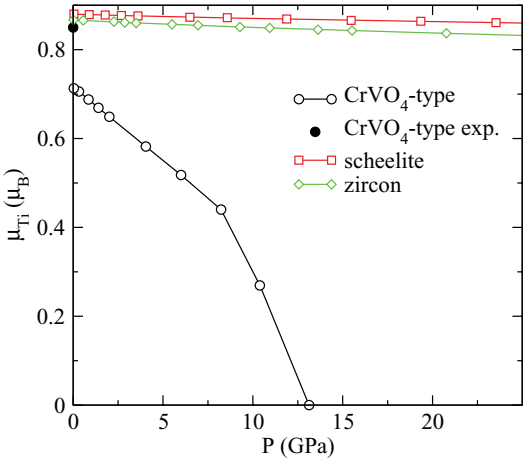

FIG. 12. (Color online) Magnetic moment, μ_{Ti}, vs pressure, P, for $TiPO_4$. Experimental data were taken from Ref. 3.

symmetry of the structure, which is reflected in the shape of the PDOS. In the case of $InPO_4$ the zone which corresponds to InO_6 tetrahedra is well defined, and in general the acoustic phonon branches have more dispersion in $TiPO_4$ than in $InPO_4$.

F. Magnetism of $TiPO_4$ under compression

Figure 12 shows the pressure evolution of the magnetic moment of Ti, μ_{Ti}, for $CrVO_4$-type, zircon, and scheelite phases of $TiPO_4$. We also have included the experimental value reported in Ref. 3 for $TiPO_4$ at ambient pressure. As can be seen, the magnetic moment of Ti from the $CrVO_4$-type structure is reduced to zero at 13 GPa. The magnetic moments of scheelite and zircon phases have very small changes in an interval of 30 GPa. On the other hand, the magnetic moment of Ti in the wolframite phase is zero.

Unfortunately there are no experimental magnetic studies performed under compression with which to compare results. The reduction of the magnetic moment induced by pressure in the $CrVO_4$-type structure is calling attention for future studies. In particular, neutron diffraction studies[65] could be performed within the pressure range of stability of the low-pressure phase to confirm our predictions.

V. SUMMARY AND CONCLUSIONS

In summary, we have studied the structural and vibrational properties of four orthophosphates, $InPO_4$, $TlPO_4$, $TiPO_4$, and VPO_4, in the $CrVO_4$-type structure. For these the Raman and IR frequencies were analyzed as functions of reduced mass. We have demonstrated by total energy calculations and lattice dynamics that the nonmagnetic phase of $TiPO_4$ is thermodynamically nonstable compared to the antiferromagnetic one.

We also study the high-pressure phase transitions for $InPO_4$ and $TiPO_4$. To do this we have used the quasiharmonic approximation to study the transitions at a temperature ≠0 K. According to our findings, at 300 K both compounds undergo the sequence phase transition $CrVO_4$ type → zircon → scheelite → wolframite. However, while the first two transitions occurs at moderate pressures (less than 20 GPa), the transition scheelite → wolframite occurs around 50 GPa.

The E vs V curves suggest that both compounds could have a further phase transition of wolframite $\rightarrow$ $SrUO_4$ type. However, the results from lattice dynamics shows that the $SrUO_4$-type phase is thermodynamically nonstable up to 90 GPa. On the other hand, we found that the wolframite phase of $InPO_4$ has a soft phonon mode between M and Γ points up to 66 GPa, which is the higher pressure studied for this phase. For $TiPO_4$, in the volframite structure, there are no imaginary phonon modes in the phonon spectrum from 59 to 68 GPa. Also, it was observed that wolframite is the less compressible phase among the others studied here. In the case of $TiPO_4$ the magnetic moment of Ti in the wolframite phase is zero.

The transition pressure, P_T, and volume contraction, ΔV, at the phase transitions of $InPO_4$ can be summarized as follows:

$$Cmcm \xrightarrow[\Delta V=-6.9\%]{P_T=6.2\ \text{GPa}} I4_1/amd \xrightarrow[-8.3]{7.5} I4_1/a \xrightarrow[-1.4]{47.8} P2/c,$$

and for $TiPO_4$

$$Cmcm \xrightarrow[\Delta V=-3.6\%]{P_T=11.1\ \text{GPa}} I4_1/amd \xrightarrow[-9.0]{18.9} I4_1/a \xrightarrow[-0.6]{49.3} P2/c.$$

As seen, the main differences among both compounds (regarding the phase transitions) is the ΔV for the first transition and the pressure range of stability for the zircon phase.

We hope the results reported here will trigger experimental studies of the interesting family of phosphates crystallizing in the CrVO4-type structure at ambient pressure.

ACKNOWLEDGMENTS

S.L.-M. acknowledges support as a UNAM fellow. D.E. acknowledges the financial support from the spanish MCYT through Grant No. MAT2010-21270-C04-01. We thank the RES (Red Española de Supercomputación) and the MALTA cluster for computer time.

*Corresponding author: lsinhue@yahoo.com.mx

[1] E. J. Baran, J. Mater. Sci. **33**, 2479 (1998).
[2] R. C. L. Mooney, Acta Crystallogr. **9**, 113 (1956).
[3] N. Kinomura, F. Muto, and M. Koizumi, J. Solid State Chem. **45**, 252 (1982).
[4] M. Touboul and K. Melghit, J. Mater. Chem. **5**, 147 (1995).
[5] L. Gracia, A. Beltrán, and D. Errandonea, Phys. Rev. B **80**, 094105 (2009).
[6] T. Yamauchi and Y. Ueda, J. Magn. Magn. Mater. **177–181**, 705 (1998).
[7] D. Errandonea and F. J. Manjón, Prog. Mater. Sci. **53**, 711 (2008).
[8] D. Errandonea, L. Gracia, A. Beltrán, A. Vegas, and Y. Meng, Phys. Rev. B **84**, 064103 (2011).
[9] D. Errandonea, R. Kumar, J. López-Solano, P. Rodríguez-Hernández, A. Muñoz, M. G. Rabie, and R. Sáez Puche, Phys. Rev. B **83**, 134109 (2011).
[10] M. Kanzaki, X. Xue, S. Reibstein, E. Berryman, and S. Namgung, Acta Crystallogr. Sect. B **67**, 30 (2011).
[11] A. K. Padhi, K. S. Nanjundaswamy, and J. B. Goodenough, J. Electrochem. Soc. **144**, 1188 (1997).
[12] S. J. Sferco, G. Allan, I. Lefebvre, M. Lannoo, E. Bergignat, and G. Hollinger, Phys. Rev. B **42**, 11232 (1990).
[13] D. Errandonea, R. Lacomba-Perales, J. Ruiz-Fuertes, A. Segura, S. N. Achary, and A. K. Tyagi, Phys. Rev. B **79**, 184104 (2009).
[14] V. Panchal, D. Errandonea, A. Segura, P. Rodriguez-Hernandez, A. Munoz, S. Lopez-Moreno, and M. Bettinelli, J. Appl. Phys. **110**, 043723 (2011).
[15] J. Ruiz-Fuertes, S. López-Moreno, D. Errandonea, J. Pellicer-Porres, R. Lacomba-Perales, A. Segura, P. Rodríguez-Hernández, A. Muñoz, A. H. Romero, and J. González, J. Appl. Phys. **107**, 083506 (2010).
[16] E. Bandiello, D. Errandonea, D. Martinez-Garcia, D. Santamaria-Perez, and F. J. Manjón, Phys. Rev. B **85**, 024108 (2012).
[17] D. Errandonea, Phys. Status Solidi B **242**, R125 (2005).
[18] D. Santamaría-Pérez, L. Gracia, G. Garbarino, A. Beltrán, R. Chuliá-Jordán, O. Gomis, D. Errandonea, C. Ferrer-Roca, D. Martínez-García, and A. Segura, Phys. Rev. B **84**, 054102 (2011).
[19] H. Sowa, J. Macavei, and H. Schultz, Z. Kristallogr. **192**, 119 (1990).
[20] S. Baroni, S. de Gironcoli, A. Dal Corso, and P. Giannozzi, Rev. Mod. Phys. **73**, 515 (2001).
[21] P. E. Blöchl, Phys. Rev. B **50**, 17953 (1994).
[22] G. Kresse and D. Joubert, Phys. Rev. B **59**, 1758 (1999).
[23] G. Kresse and J. Hafner, Phys. Rev. B **47**, 558 (1993).
[24] G. Kresse and J. Hafner, Phys. Rev. B **49**, 14251 (1994).
[25] G. Kresse and J. Furthmüller, Comput. Mater. Sci. **6**, 15 (1996).
[26] G. Kresse and J. Furthmüller, Phys. Rev. B **54**, 11169 (1996).
[27] J. P. Perdew, K. Burke, and M. Ernzerhof, Phys. Rev. Lett. **77**, 3865 (1996).
[28] J. P. Perdew, K. Burke, and M. Ernzerhof, Phys. Rev. Lett. **78**, 1396 (1997).
[29] R. Armiento and A. E. Mattsson, Phys. Rev. B **72**, 085108 (2005).
[30] A. E. Mattsson and R. Armiento, Phys. Rev. B **79**, 155101 (2009).
[31] A. E. Mattsson, R. Armiento, J. Paier, G. Kresse, J. M. Wills, and T. R. Mattsson, J. Chem. Phys. **128**, 084714 (2008).
[32] J. P. Perdew, A. Ruzsinszky, G. I. Csonka, O. A. Vydrov, G. E. Scuseria, L. A. Constantin, X. Zhou, and K. Burke, Phys. Rev. Lett. **100**, 136406 (2008).
[33] J. P. Perdew, A. Ruzsinszky, G. I. Csonka, O. A. Vydrov, G. E. Scuseria, L. A. Constantin, X. Zhou, and K. Burke, Phys. Rev. Lett. **102**, 039902(E) (2009).
[34] J. M. Law, C. Hoch, R. Glaum, I. Heinmaa, R. Stern, J. Kang, C. Lee, M.-H. Whangbo, and R. K. Kremer, Phys. Rev. B **83**, 180414 (2011).
[35] R. Glaum, M. Reehuis, N. Stuber, U. Kaiser, and F. Reinauer, J. Solid State Chem. **126**, 15 (1996).
[36] J. López-Solano, P. Rodríguez-Hernández, A. Muñoz, O. Gomis, D. Santamaría-Perez, D. Errandonea, F. J. Manjón, R. S. Kumar, E. Stavrou, and C. Raptis, Phys. Rev. B **81**, 144126 (2010).
[37] H. J. Monkhorst and J. D. Pack, Phys. Rev. B **13**, 5188 (1976).
[38] K. Parlinski, computer code PHONON. See http://wolf.ifj.edu.pl/phonon.
[39] A. Leclaire, A. Benmoussa, M. M. Borel, A. Grandin, and B. Raveau, Eur. J. Solid State Inorg. Chem. **28**, 1323 (1991).
[40] V. Peltier, P. Deniard, R. Brec, and R. Marchand, C. R. Chim. **1**, 57 (1998).

[41]M. Weil, Acta Crystallogr. Sect. E **63**, i172 (2007).
[42]S. López-Moreno, P. Rodríguez-Hernández, A. Muñoz, A. H. Romero, and D. Errandonea, Phys. Rev. B **84**, 064108 (2011).
[43]J. Ruiz-Fuertes, D. Errandonea, S. López-Moreno, J. González, O. Gomis, R. Vilaplana, F. J. Manjón, A. Muñoz, P. Rodríguez-Hernández, A. Friedrich, I. A. Tupitsyna, and L. L. Nagornaya, Phys. Rev. B **83**, 214112 (2011).
[44]J. Ruiz-Fuertes, S. López-Moreno, J. López-Solano, D. Errandonea, A. Segura, R. Lacomba-Perales, A. Muñoz, S. Radescu, P. Rodríguez-Hernández, M. Gospodinov, L. L. Nagornaya, and C. Y. Tu, Phys. Rev. B **86**, 125202 (2012).
[45]A. P. Young and C. M. Schwartz, Acta Crystallogr. **15**, 1305 (1962).
[46]D. Errandonea, R. Kumar, J. López-Solano, P. Rodríguez-Hernández, A. Muñoz, M. G. Rabie, and R. Sáez Puche, Phys. Rev. B **83**, 134109 (2011).
[47]L. Gracia, A. Beltrán, D. Errandonea, and J. Andrés, Inorg. Chem. **51**, 1751 (2012).
[48]G. Korotcenkov, I. Boris, A. Cornet, J. Rodriguez, A. Cirera, V. Golovanov, Y. Lychkovsky, and G. Karkotsky, Sens. Actuators B **120**, 657 (2007).
[49]M. Rojas-López, J. Nieto-Navarro, E. Rosendo, H. Navarro-Contreras, and M. Vidal, Thin Solid Films **379**, 1 (2000).
[50]E. J. Baran, F. Muto, N. Kumada, and N. Kinomura, J. Mater. Sci. Lett. **8**, 1305 (1989).
[51]F. Birch, Phys. Rev. **71**, 809 (1947).
[52]S. López-Moreno and D. Errandonea (unpublished).
[53]A. Mujica, A. Rubio, A. Muñoz, and R. J. Needs, Rev. Mod. Phys. **75**, 863 (2003).
[54]G. P. Schwartz, W. A. Sunder, and J. E. Griffiths, Appl. Phys. Lett. **37**, 925 (1980).
[55]B. A. Kolesov, C. A. Geiger, and T. Armbruster, Eur. J. Mineral. **13**, 939 (2001).
[56]V. Panchal, S. López-Moreno, D. Santamaría-Pérez, D. Errandonea, F. J. Manjón, P. Rodríguez-Hernandez, A. Muñoz, S. N. Achary, and A. K. Tyagi, Phys. Rev. B **84**, 024111 (2011).
[57]R. Lacomba-Perales, D. Errandonea, Y. Meng, and M. Bettinelli, Phys. Rev. B **81**, 064113 (2010).
[58]E. Stavrou, A. Tatsi, C. Raptis, I. Efthimiopoulos, K. Syassen, A. Muñoz, P. Rodríguez-Hernández, J. López-Solano, and M. Hanfland, Phys. Rev. B **85**, 024117 (2012).
[59]R. Lacomba-Perales, D. Errandonea, D. Martinez-Garcia, P. Rodríguez-Hernández, S. Radescu, A. Mujica, A. Muñoz, J. C. Chervin, and A. Polian, Phys. Rev. B **79**, 094105 (2009).
[60]V. Panchal, F. J. Manjón, D. Errandonea, P. Rodriguez-Hernandez, J. López-Solano, A. Muñoz, S. N. Achary, and A. K. Tyagi, Phys. Rev. B **83**, 064111 (2011).
[61]D. Errandonea and F. J. Manjón, Mater. Res. Bull. **44**, 807 (2009).
[62]E. Stavrou, I. Efthimiopoulos, S. M. Souliou, J. Law, R. K. Kremer, G. V. Vajenine, K. Syassen, and M. Hanfland, Acta Crystallogr. Sect. A **66**, s48 (2010).
[63]S. López-Moreno, A. H. Romero, P. Rodríguez-Hernández, and A. Muñoz, High Press. Res. **29**, 578 (2009).
[64]D. Errandonea, F. J. Manjón, N. Garro, P. Rodríguez-Hernández, S. Radescu, A. Mujica, A. Muñoz, and C. Y. Tu, Phys. Rev. B **78**, 054116 (2008).
[65]H. Ehrenberg, M. Wiesmann, J. Garcia-Jaca, H. Weitzel, and H. Fuess, J. Magn. Magn. Mater. **182**, 152 (1998).